Gate-Tunable Band Structure of the LaAlO₃-SrTiO₃ Interface

A. E. M. Smink, J. C. de Boer, M. P. Stehno, A. Brinkman, W. G. van der Wiel, and H. Hilgenkamp

MESA+ Institute for Nanotechnology, University of Twente, P.O. Box 217, 7500 AE Enschede, The Netherlands

(Received 10 October 2016; published 6 March 2017)

The two-dimensional electron system at the interface between LaAlO₃ and SrTiO₃ has several unique properties that can be tuned by an externally applied gate voltage. In this work, we show that this gate tunability extends to the effective band structure of the system. We combine a magnetotransport study on top-gated Hall bars with self-consistent Schrödinger-Poisson calculations and observe a Lifshitz transition at a density of $2.9 \times 10^{13} \mathrm{cm}^{-2}$. Above the transition, the carrier density of one of the conducting bands decreases with increasing gate voltage. This surprising decrease is accurately reproduced in the calculations if electronic correlations are included. These results provide a clear, intuitive picture of the physics governing the electronic structure at complex-oxide interfaces.

The two-dimensional electron system (2DES) at the interface between the band insulators LaAlO₃ (LAO) and SrTiO₃ (STO) displays many intriguing phenomena, which may be harnessed for novel electronic devices [1–5]. The discovery of superconductivity [6], magnetic signatures [7–10], and their apparent coexistence [11] sparked growing interest in this material system. These properties can be tuned by varying parameters during growth [4,7], as well as by an externally applied electric field after growth [12]. Using this field effect, control of superconductivity [13–17], of spin-orbit coupling [17–20], and of carrier mobility [21,22] has been reported. Recent progress on local control of superconductivity [16] opened a route towards electrically controlled oxide Josephson junctions [23,24], providing new opportunities for superconducting electronic devices. Because these phenomena are related to the interfacial band structure, a fundamental understanding of the band structure is vital for the understanding of these phenomena and their exploitation in electronic devices.

The interface band structure is formed by the conduction band of STO, which is bent down at the interface and crosses the Fermi level [25]. The origin of the band bending is still an open question [26–28]. This band bending creates a potential well, confining the carriers to a few nanometers in the out-of-plane direction [29–32]. In the well, the effective band structure is formed by the Ti t_{2g} orbitals. For interfaces grown along the [001] direction, the in-plane oriented d_{xy} bands lie below the out-of-plane oriented $d_{yz,xz}$ bands in energy due to the confinement, as measured using x-ray absorption [33].

By backgating the interface through the STO substrate, an additional conduction channel was observed to emerge above a carrier density of $(1.7 \pm 0.1) \times 10^{13}$ cm^{-2} [34]. This observation was linked to tuning the Fermi level across the bottom of the $d_{yz,xz}$ bands, making additional electron pockets available for conduction. As a result, the

Fermi surface topology changes, which is the characteristic feature of a Lifshitz transition [35].

The model proposed by Joshua *et al.* [34] implied a set of band structure parameters that may not apply in general. Subsequent experiments using a (backgate-assisted) top-gating setup were not able to reproduce the Lifshitz transition scenario [16,20,22,36]. In these studies, a carrier density up to 2.5×10^{13} cm^{-2} was reported, i.e., well above the density of the Lifshitz transition mentioned above. This suggests that the Lifshitz transition does not occur at a fixed carrier density, but depends crucially on the electrostatic boundary conditions among other parameters.

In this Letter, we report top-gating experiments on LAO-STO interface devices over a wide gate voltage range with low gate-leakage currents. From two-band fits on the magnetotransport data, we extract the evolution of the d_{xy} and $d_{yz,xz}$ carrier densities with top-gate voltage. By self-consistent Schrödinger-Poisson calculations, we provide a simple, intuitive picture of the band structure of the 2DES, which crucially depends on out-of-plane electrostatics. This approach naturally explains our observation of a Lifshitz transition at a carrier density of $(2.9 \pm 0.1) \times 10^{13}$ cm^{-2}, almost twice the value reported for backgating. Above the transition, we observe a reduction of the d_{xy} carrier density with gate voltage, which can be attributed to electron-electron interactions.

To study the top-gate dependence of the transport parameters, several Hall bars were fabricated on SrTiO₃ substrates, which were TiO₂-terminated by etching in buffered hydrofluoric acid (BHF) [37]. Subsequently, a ~20 nm thick amorphous AlO$_x$ layer was deposited and Hall bar structures were defined through photolithography and etching in a base [38]. These Hall bars are 30–100 μm wide and 400 μm long. After structuring, 10 unit cells (u.c.) of LaAlO₃ were deposited using pulsed laser deposition at 850 °C and an oxygen pressure of 5×10^{-5} mbar, with a laser fluence of 1.3 J cm^{-2} and spot size of 1.76 mm². The
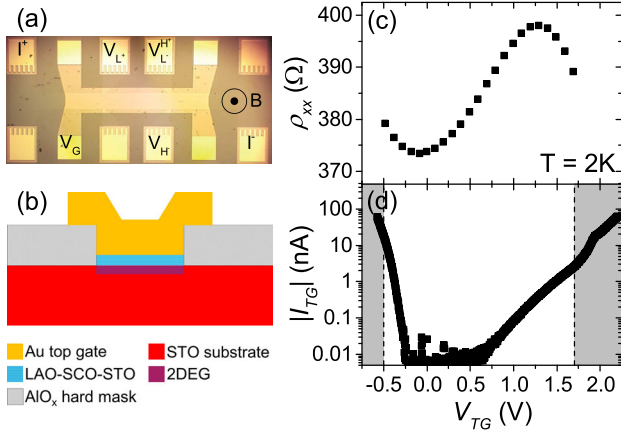
FIG. 1.   Device layout and basic electrical properties. (a) Optical micrograph of a 75-μm-wide Hall bar with electrical connections and magnetic field direction indicated. (b) Schematic cross section of device. (c) Sheet resistance and (d) absolute gate leakage current as a function of top-gate voltage at $T = 2$ K and $B = 0$ T. The shaded area is excluded for further analysis due to conditions discussed in the main text.

target-substrate distance was 45 mm. To suppress formation of oxygen vacancies, the film was capped *in situ* with 1 u.c. of $SrCuO_2$ and 2 u.c. of $SrTiO_3$, at 600 °C and in 6×10^{-2} mbar of oxygen [39]. The sample was then cooled down to room temperature at 10 °C/min in deposition pressure and transferred *ex situ* to a sputtering chamber. There, a 30 nm thick Au layer was deposited at a low rate of ~ 1 nm/min in 8×10^{-2} mbar of argon gas. Au/Ti contact pads were deposited in another sputtering step, after which the gate electrodes were defined by etching in a buffered KI solution. A photograph and a schematic of the device are shown in Figs. 1(a)–1(b). The top-gate voltage V_{TG} was applied between the gate electrode, V_G, and the source, I^-. We measured several devices on two different samples showing similar behavior. In the following, we discuss results for one of these devices.

The gate leakage current, $I_{TG}(V_{TG})$, depicted in Fig. 1(d) is very small compared to values reported in the literature [16,22,40], given the size of the gated area: $\sim 4 \times 10^4$ μm^2. This indicates that the dielectric of our samples is an excellent insulator, which can be ascribed to the gentle metal deposition and/or to the $SrCuO_2$ capping. The effect of the latter would be enhanced oxygen uptake [39] and a small defect density in the overlayer. For the transport measurements, we chose the gate voltage range between -0.5 V and $+1.7$ V. In this range, two requirements are met: the gate leakage current is maximally 1% of the excitation current, and no dielectric breakdown is observed. We interpret the upturn of I_{TG} above $V_{TG} = +1.7$ V as an onset of break-down, as the corresponding electric field is $\gtrsim 3.5$ MV cm^{-1}.

Within this range, the resistivity depends on the top-gate voltage in a nontrivial way, as depicted in Fig. 1(c). The behavior on the left-hand side ($V_{TG} \lesssim 0.5$ V) can be explained by opposite trends in the density and mobility of the charge carriers with gate voltage [22], whereas the right-hand side requires additional explanation. To shed light on the origin of this unusual gate dependence of the resistivity, magnetoresistance measurements were performed in 100 mV gate voltage steps. The results are depicted in Figs. 2(a)–2(c). Besides low-field signatures of weak antilocalization [18], we observe the characteristic features attributed to a Lifshitz transition in the band structure of the LAO-STO interface [34]: the emerging positive magnetoresistance, nonlinear Hall signal, and an upturn of the low-field Hall slope. However, the character-istic changes all occur at different gate voltages.

To extract the carrier density as a function of gate voltage, we inverted the 2D resistivity matrix to obtain the conduc-tivity in longitudinal (σ_{xx}) and transverse (σ_{xy}) direction as a function of magnetic field, plotted in Figs. 2(d)–2(e). For every top-gate voltage, a two-band conduction model was made to fit these curves simultaneously:

$$\sigma_{xx} = e \sum_{i=1,2} \frac{n_i \mu_i}{1+(\mu_i B)^2}; \quad \sigma_{xy} = eB \sum_{i=1,2} \frac{n_i \mu_i^2}{1+(\mu_i B)^2}, \quad (1)$$

where n_i is the carrier density and μ_i the mobility of the ith band, and $B = \mu_0 H$ is the magnetic field. For fitting through the Lifshitz transition, we assume continuity of n_1 and n_2. This corresponds to requiring the Fermi surface area to be continuous as a function of chemical potential. This con-dition can be met by assuming a lower limit for the mobility of the second band, μ_2, just above the transition. This avoids n_2 to diverge as the Lifshitz transition is approached from high gate voltages downwards. Figure 3 presents the extracted carrier density as a function of gate voltage; the corresponding mobility values are discussed in the Supplemental Material [41].

Compared to previous studies on top-gating of the interface [16,20,22,36], we can tune the carrier density to much higher values owing to the low gate-leakage current. In the range that overlaps with the tuning range of these previous studies, i.e., $n_{tot} \lesssim 2.5 \times 10^{13}$ cm^{-2}, the resistance decreases with increasing carrier density. In the extended range, we observe most notably the emergence of a second mobile carrier type around a carrier density of $(2.9 \pm 0.1) \times 10^{13}$ cm^{-2}. We interpret this as the Lifshitz density n_L of this sample. In the following, as only d_{xy} states are available below n_L, we consider the experimen-tally found n_1 to be of d_{xy} character and n_2 to represent the $d_{yz,xz}$ states. Since this Lifshitz density is almost twice the value of Ref. [34], the energy offset between the d_{xy} and $d_{xz,yz}$ bands is evidently larger. This means that the effective band structure in the two cases must differ.

Our second observation is the decrease of d_{xy} carrier density with increasing gate voltage above the Lifshitz transition. Such a decrease is incompatible with a model requiring a fixed electronic band structure, as raising the
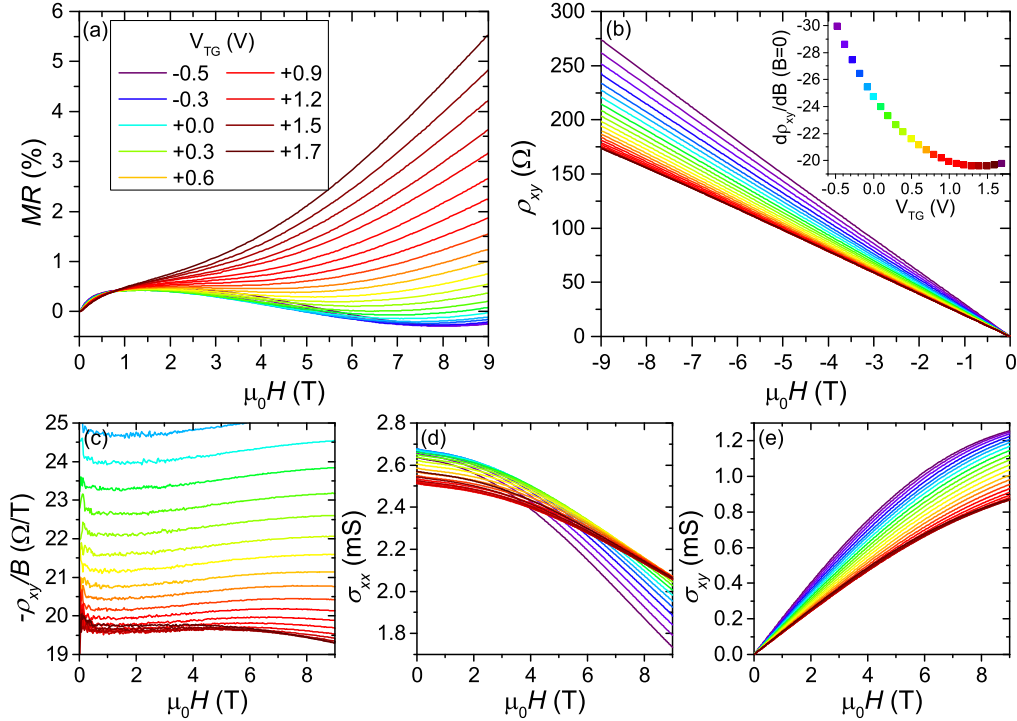
FIG. 2.   Magnetotransport curves after symmetrization at $T = 2$ K. (a) Magnetoresistance MR $= [\rho_{xx}(B)/\rho_{xx}(0) - 1] \times 100\%$ showing positive magnetoresistance for $V_{TG} \gtrsim +0.3$ V. The legend applies to all graphs. (b) Hall resistance showing an emerging slight nonlinearity around $V_{TG} \sim +1.2$ V. The inset shows the zero-field slope, with an upturn above $V_{TG} = +1.3$ V. (c) Hall coefficient, where the nonlinearity in the Hall resistance is more visible as the signal starts turning downwards with field with increasing gate voltage. (d) Longitudinal and (e) Hall conductivity used for fitting the two-band model described in the text.

Fermi energy should always increase the number of available conduction states up to the point where the band is full. This is not the case here. Instead, it appears that the carriers redistribute to the $d_{yz,xz}$ bands. This indicates that the effective band structure is not fixed, but evolves with gate voltage. Below, we discuss these two observations using self-consistent Schrödinger-Poisson calculations [42].

For these calculations, we follow the methods of Refs. [43,44] and use the effective mass and envelope wave function approximations. By the orbital orientation, the effective masses are low along the orbital lobes and high perpendicular to them. So, for the d_{xy} orbital, $m^* = m_l$ in the x and y directions and $m^* = m_h$ in the z direction. We take the effective masses as $m_l = 0.7 \, m_e$ and $m_h = 14 \, m_e$ [44,45]. The result of this effective mass anisotropy in a confined system is to lift the bulk degeneracy of the bands [33]. In the Schrödinger-Poisson approach, this follows naturally from the $\hbar^2/2m^*$ prefactor in the Hamiltonian: since the d_{xy} band has a higher effective mass out of plane, it lies lower in energy. The Schrödinger equation also dictates that as a potential well becomes narrower, the energy of the states increases. Since this is mediated by the prefactor $\hbar/2m^*$, the d_{xy} energy will increase slower than the energy of the $d_{xz,yz}$ states. This leads to the conclusion that in our experiment, the potential well at the Lifshitz point is narrower than it was in the backgate experiment [34].

Considerations of the electrostatic effects of a gate voltage support this conclusion. Besides inducing carriers through capacitive coupling, the gate-induced electric field affects the potential well, which can itself be described as an integrated electric field. The potential well is usually modeled by implying an infinite energy barrier on the LAO side of the interface, and defined relative to the conduction band minimum in the STO bulk [43,44]. Taking $z > 0$ to be
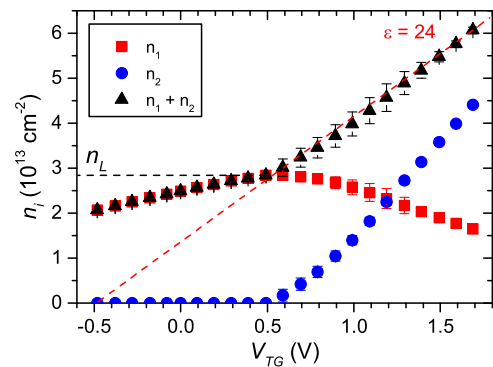

FIG. 3.   Carrier density versus top-gate voltage and $T = 2$ K, specified per carrier type by the two-band fitting model described in the text. The black dashed line indicates the Lifshitz carrier density. The red line is the slope of the carrier density calculated from a parallel-plate capacitor model with $\epsilon = 24$ and $d = 5$ nm.

the STO side of the interface, the electric field resulting from a positive top-gate voltage has a positive sign and a positive backgate voltage results in a negative electric field. Besides the primary effect of doping more carriers, which by the Poisson equation narrows the potential well, the second-order effect of the gating geometries is opposite: a positive top-gate (backgate) voltage enhances (weakens) the confining potential gradient, resulting in a larger splitting in energy in the top-gate case.

For the calculations, we assume that the potential well is formed by the mobile carriers n_m and a bound background charge n_b spread homogeneously across a thickness of 100 nm. We assume n_b to originate from defect levels deep in the STO gap, and thus independent of the gate voltage. Then, a gate voltage only tunes n_m. In each iteration step, we evaluate the electric-field dependent permittivity ϵ_r of SrTiO$_3$, using the dependence of Ref. [43] with $\epsilon_\infty = 6$ [46]. Choosing a different function for $\epsilon_r(E)$, e.g., from Refs. [32,46], does not affect the qualitative results, but influences the quantitative outcomes. In the model, we vary n_m and n_b to study the occupancy of the d_{xy} and $d_{yz,xz}$ states. Importantly, a change in n_b influences the Lifshitz density as this alters the shape of the potential well. By choosing $n_b = 8.3 \times 10^{18}$ cm^{-3}, the calculations reproduce the experimentally found Lifshitz density. Other values for the effective masses that are reported in the literature, e.g., Refs. [47,48], require choosing a different background charge density.

The results of the SP calculation are given by the open symbols and dashed lines in Fig. 4(a), which clearly does not reproduce the decrease of n_1. The redistribution of carriers to the $d_{yz,xz}$ bands can thus not be explained by interaction of the potential well and the band structure alone, but has to be mediated by an effect not yet included in the calculations. As recently reported by Maniv *et al.* [49], electronic correlations can mediate such a redistribution of carriers.

We model these correlations as repulsive electron-electron interactions, with an interaction term $E_{\text{int}}^i = \sum_{j=1}^n U(1 - \delta_{ij}/2)N_j$, for each band i [49]. Here, N_j is the 2D electron density per unit cell of band j, δ_{ij} is the Kronecker delta, and U is the phenomenological screened Coulomb interaction strength between bands, which we take equal for all bands for simplicity. The Kronecker delta term is included to avoid unphysical self-interactions. We include this interaction term in the self-consistent band occupancy calculation in the SP model.

Using $U = 1.65$ eV and $n_b = 6.9 \times 10^{18}$ cm^{-3}, the evolution of n_1 and n_2 is calculated as the solid lines in Fig. 4(a), closely resembling the experimental data. The resulting band structures for $n \ll n_L$, $n = n_L$, and $n \gg n_L$ are given in Figs. 4(b)–4(d), respectively. From these calculations, it becomes clear that the net effect of this electron-electron interaction is to shift bands with low density of states (DOS) up in energy with respect to the bands with high DOS, once the latter are occupied. A second effect of the
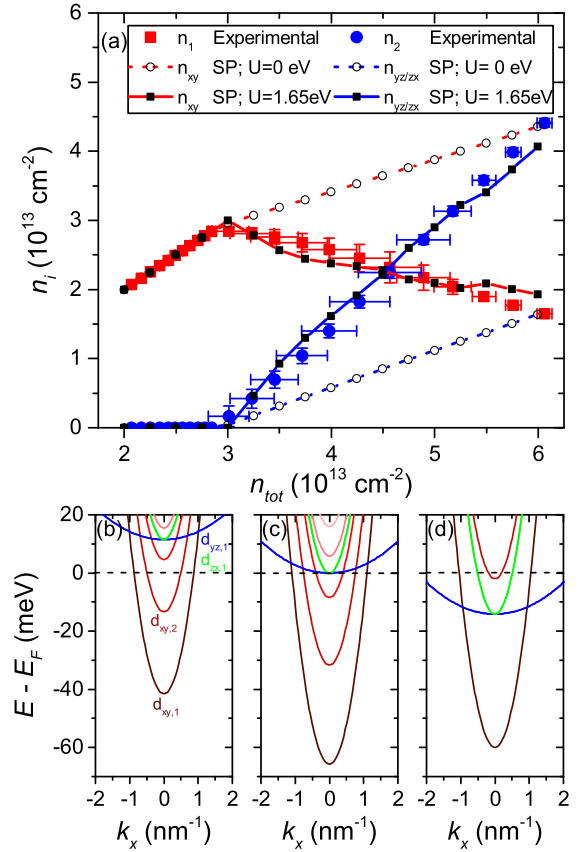

FIG. 4. Results of the self-consistent Schrödinger-Poisson calculations. (a) Calculated and measured carrier density per band versus the total carrier density. The symbols with error bars represent the experimental values; the symbols with connecting lines (as guide to the eye) correspond to calculated values by the Schrödinger-Poisson model as described in the text. Dashed lines (open symbols) represent calculations without electron-electron interactions, solid lines are calculated with $U = 1.65$ eV. (b)–(d) Calculated band structures including electron-electron interactions for (b) $n_{\text{tot}} \ll n_L$, (c) $n_{\text{tot}} = n_L$, and (d) $n_{\text{tot}} \gg n_L$. The horizontal dashed line represents the Fermi energy and the color legend in (b) applies to all panels.

electron-electron interaction surfaces when the chemical potential μ is calculated following Ref. [44]: U makes μ increase with gating above the Lifshitz transition. Although our calculations also show a slight decrease of μ versus n_{tot} just above the Lifshitz transition, which should result in electronic phase separation according to Ref. [44], phase separation alone is not enough to explain the observed decrease of n_1 with gating. Without electron-electron interaction, even in the high-density puddles, the d_{xy} density would never become smaller than the $d_{xz,yz}$ density, as follows from the dashed lines in Fig. 4(a).

In summary, we have observed a Lifshitz transition in the band structure of the LaAlO$_3$ − SrTiO$_3$ interface at a carrier density of $(2.9 \pm 0.1) \times 10^{13}$ cm^{-2}. Above the transition, the density of d_{xy}-type charge carriers decreases with increasing gate voltage. To investigate this behavior, we

performed self-consistent band structure calculations by solving the coupled Schrödinger and Poisson equations. The obtained band occupations are in excellent agreement with the experimental data when an electron-electron interaction term is included in the model. This term mediates a shift in d_{xy} subbands when $d_{yz,xz}$ subbands become occupied.

Based on these observations, we conclude that electrostatics and electronic correlations are equally important factors governing the band structure of $SrTiO_3$-based two-dimensional electron systems. The growth conditions of the polar oxide, dopants, and oxygen deficiency in the $SrTiO_3$ substrate, and the presence of a metallic top-gate electrode determine the shape of the potential well at low carrier concentrations. Once the heavier $d_{yz,xz}$ bands are populated, electron-electron interactions wield influence on the relative band occupations. Therefore, the relative band offsets of the Ti t_{2g} bands and the carrier density of the Lifshitz transition, associated with the occupation of bands of out-of-plane orbitals, should not be considered fixed, but they evolve with the shape of the potential well.

An improved understanding of the band structure at complex oxide interfaces is an important step in the direction of a universal framework that explains the unusual gate dependence of carrier mobility, spin-orbit coupling, and superconductivity in these systems. However, progress toward this goal will go beyond electrostatic control of the carrier density and will require careful engineering of the well shape using optimized growth and doping techniques.

[1] A. Ohtomo and H. Y. Hwang, Nature (London) **427**, 423 (2004).

[2] J. Mannhart and D. G. Schlom, Science **327**, 1607 (2010).

[3] H. Y. Hwang, Y. Iwasa, M. Kawasaki, B. Keimer, N. Nagaosa, and Y. Tokura, Nat. Mater. **11**, 103 (2012).

[4] Y.-W. Xie and H. Y. Hwang, Chin. Phys. B **22**, 127301 (2013).

[5] H. Hilgenkamp, MRS Bull. **38**, 1026 (2013).

[6] N. Reyren, S. Thiel, A. D. Caviglia, L. F. Kourkoutis, G. Hammerl, C. Richter, C. W. Schneider, T. Kopp, A.-S. Retschi, D. Jaccard, M. Gabay, D. A. Muller, J.-M. Triscone, and J. Mannhart, Science **317**, 1196 (2007).

[7] A. Brinkman, M. Huijben, M. van Zalk, J. Huijben, U. Zeitler, J. C. Maan, W. G. van der Wiel, G. Rijnders, D. H. A. Blank, and H. Hilgenkamp, Nat. Mater. **6**, 493 (2007).

[8] Ariando, X. Wang, G. Baskaran, Z. Q. Liu, J. Huijben, J. B. Yi, A. Annadi, A. R. Barman, A. Rusydi, S. Dhar, Y. P. Feng, J. Ding, H. Hilgenkamp, and T. Venkatesan, Nat. Commun. **2**, 188 (2011).

[9] J.-S. Lee, Y. W. Xie, H. K. Sato, C. Bell, Y. Hikita, H. Y. Hwang, and C.-C. Kao, Nat. Mater. **12**, 703 (2013).

[10] S. Banerjee, O. Erten, and M. Randeria, Nat. Phys. **9**, 626 (2013).

[11] L. Li, C. Richter, J. Mannhart, and R. C. Ashoori, Nat. Phys. **7**, 762 (2011).

[12] S. Thiel, G. Hammerl, A. Schmehl, C. W. Schneider, and J. Mannhart, Science **313**, 1942 (2006).

[13] A. D. Caviglia, S. Gariglio, N. Reyren, D. Jaccard, T. Schneider, M. Gabay, S. Thiel, G. Hammerl, J. Mannhart, and J.-M. Triscone, Nature (London) **456**, 624 (2008).

[14] J. Biscaras, N. Bergeal, S. Hurand, C. Grossetete, A. Rastogi, R. C. Budhani, D. LeBoeuf, C. Proust, and J. Lesueur, Phys. Rev. Lett. **108**, 247004 (2012).

[15] C. Richter, H. Boschker, W. Dietsche, E. Fillis-Tsirakis, R. Jany, F. Loder, L. F. Kourkoutis, D. A. Muller, J. R. Kirtley, C. W. Schneider, and J. Mannhart, Nature (London) **502**, 528 (2013).

[16] P. D. Eerkes, W. G. van der Wiel, and H. Hilgenkamp, Appl. Phys. Lett. **103**, 201603 (2013).

[17] M. Ben Shalom, M. Sachs, D. Rakhmilevitch, A. Palevski, and Y. Dagan, Phys. Rev. Lett. **104**, 126802 (2010).

[18] A. D. Caviglia, M. Gabay, S. Gariglio, N. Reyren, C. Cancellieri, and J.-M. Triscone, Phys. Rev. Lett. **104**, 126803 (2010).

[19] D. Stornaiuolo, S. Gariglio, A. Fête, M. Gabay, D. Li, D. Massarotti, and J.-M. Triscone, Phys. Rev. B **90**, 235426 (2014).

[20] S. Hurand, A. Jouan, C. Feuillet-Palma, G. Singh, J. Biscaras, E. Lesne, N. Reyren, A. Barthélémy, M. Bibes, J. E. Villegas, C. Ulysse, X. Lafosse, M. Pannetier-Lecoeur, S. Caprara, M. Grilli, J. Lesueur, and N. Bergeal, Sci. Rep. **5**, 12751 (2015).

[21] C. Bell, S. Harashima, Y. Kozuka, M. Kim, B. G. Kim, Y. Hikita, and H. Y. Hwang, Phys. Rev. Lett. **103**, 226802 (2009).

[22] M. Hosoda, Y. Hikita, H. Y. Hwang, and C. Bell, Appl. Phys. Lett. **103**, 103507 (2013).

[23] S. Goswami, E. Mulazimoglu, L. M. K. Vandersypen, and A. D. Caviglia, Nano Lett. **15**, 2627 (2015).

[24] S. Goswami, E. Mulazimoglu, A. M. R. V. L. Monteiro, R. Wölbing, D. Koelle, R. Kleiner, Y. M. Blanter, L. M. K. Vandersypen, and A. D. Caviglia, Nat. Nanotechnol. **11**, 861 (2016).

[25] Z. S. Popović, S. Satpathy, and R. M. Martin, Phys. Rev. Lett. **101**, 256801 (2008).

[26] N. Nakagawa, H. Y. Hwang, and D. A. Muller, Nat. Mater. **5**, 204 (2006).

[27] W. Siemons, G. Koster, H. Yamamoto, W. A. Harrison, G. Lucovsky, T. H. Geballe, D. H. A. Blank, and M. R. Beasley, Phys. Rev. Lett. **98**, 196802 (2007).

[28] L. Yu and A. Zunger, Nat. Commun. **5**, 5118 (2014).

[29] M. Basletic, J.-L. Maurice, C. Carrétéro, G. Herranz, O. Copie, M. Bibes, E. Jacquet, K. Bouzehouane, S. Fusil, and A. Barthélémy, Nat. Mater. **7**, 621 (2008).

[30] M. Sing, G. Berner, K. Goß, A. Müller, A. Ruff, A. Wetscherek, S. Thiel, J. Mannhart, S. A. Pauli, C. W.

Schneider, P. R. Willmott, M. Gorgoi, F. Schäfers, and R. Claessen, Phys. Rev. Lett. **102**, 176805 (2009).

[31] N. Reyren, S. Gariglio, A. D. Caviglia, D. Jaccard, T. Schneider, and J.-M. Triscone, Appl. Phys. Lett. **94**, 112506 (2009).

[32] O. Copie, V. Garcia, C. Bödefeld, C. Carrétéro, M. Bibes, G. Herranz, E. Jacquet, J.-L. Maurice, B. Vinter, S. Fusil, K. Bouzehouane, H. Jaffrès, and A. Barthélémy, Phys. Rev. Lett. **102**, 216804 (2009).

[33] M. Salluzzo, J. C. Cezar, N. B. Brookes, V. Bisogni, G. De Luca, C. Richter, S. Thiel, J. Mannhart, M. Huijben, A. Brinkman, G. Rijnders, and G. Ghiringhelli, Phys. Rev. Lett. **102**, 166804 (2009).

[34] A. Joshua, S. Pecker, J. Ruhman, E. Altman, and S. Ilani, Nat. Commun. **3**, 1129 (2012).

[35] Y. Yamaji, T. Misawa, and M. Imada, J. Phys. Soc. Jpn. **75**, 094719 (2006).

[36] W. Liu, S. Gariglio, A. Fête, D. Li, M. Boselli, D. Stornaiuolo, and J.-M. Triscone, APL Mater. **3**, 062805 (2015).

[37] G. Koster, B. L. Kropman, G. J. H. M. Rijnders, D. H. A. Blank, and H. Rogalla, Appl. Phys. Lett. **73**, 2920 (1998).

[38] N. Banerjee, M. Huijben, G. Koster, and G. Rijnders, Appl. Phys. Lett. **100**, 041601 (2012).

[39] M. Huijben, G. Koster, M. K. Kruize, S. Wenderich, J. Verbeeck, S. Bals, E. Slooten, B. Shi, H. J. A. Molegraaf, J. E. Kleibeuker, S. van Aert, J. B. Goedkoop, A. Brinkman, D. H. A. Blank, M. S. Golden, G. van Tendeloo, H. Hilgenkamp, and G. Rijnders, Adv. Funct. Mater. **23**, 5240 (2013).

[40] C. Woltmann, T. Harada, H. Boschker, V. Srot, P. van Aken, H. Klauk, and J. Mannhart, Phys. Rev. Applied **4**, 064003 (2015).

[41] See Supplemental Material at http://link.aps.org/supplemental/10.1103/PhysRevLett.118.106401 for the results of fitting for the carrier mobility, and for a discussion of its dependence on the top-gate voltage.

[42] F. Stern, Phys. Rev. B **5**, 4891 (1972).

[43] S. Gariglio, A. Fête, and J.-M. Triscone, J. Phys. Condens. Matter **27**, 283201 (2015).

[44] N. Scopigno, D. Bucheli, S. Caprara, J. Biscaras, N. Bergeal, J. Lesueur, and M. Grilli, Phys. Rev. Lett. **116**, 026804 (2016).

[45] A. F. Santander-Syro, O. Copie, T. Kondo, F. Fortuna, S. Pailhès, R. Weht, X. G. Qiu, F. Bertran, A. Nicolaou, A. Taleb-Ibrahimi, P. Le Fèvre, G. Herranz, M. Bibes, N. Reyren, Y. Apertet, P. Lecoeur, A. Barthélémy, and M. J. Rozenberg, Nature (London) **469**, 189 (2011).

[46] R. C. Neville, B. Hoeneisen, and C. A. Mead, J. Appl. Phys. **43**, 2124 (1972).

[47] Z. Zhong, A. Tóth, and K. Held, Phys. Rev. B **87**, 161102 (R) (2013).

[48] A. McCollam, S. Wenderich, M. K. Kruize, V. K. Guduru, H. J. A. Molegraaf, M. Huijben, G. Koster, D. H. A. Blank, G. Rijnders, A. Brinkman, H. Hilgenkamp, U. Zeitler, and J. C. Maan, APL Mater. **2**, 022102 (2014).

[49] E. Maniv, M. B. Shalom, A. Ron, M. Mograbi, A. Palevski, M. Goldstein, and Y. Dagan, Nat. Commun. **6**, 8239 (2015).